ROYAL SOCIETY
OF CHEMISTRY

Check for updates

Observing quantum trapping on MoS$_2$ through the lifetimes of resonant electrons: revealing the Pauli exclusion principle†

Wei-Bin Su, [ID] *[a] Shin-Ming Lu, [ID] [a] Horng-Tay Jeng, [ID] *[bac] Wen-Yuan Chan,[a] Ho-Hsiang Chang,[a] Woei Wu Pai,[d] Hsiang-Lin Liu [ID] [e] and Chia-Seng Chang[a]

We demonstrate that the linewidth of the field emission resonance (FER) observed on the surface of MoS$_2$ using scanning tunneling microscopy can vary by up to one order of magnitude with an increasing electric field. This phenomenon originates from quantum trapping, in which the electron relaxed from a resonant electron in the FER is momentarily trapped in a potential well on the MoS$_2$ surface due to its wave nature. Because the relaxed electron and the resonant electron have the same spin, through the action of the Pauli exclusion principle, the lifetimes of the resonant electrons can be substantially prolonged when the relaxed electrons engage in resonance trapping. The linewidth of the FER is thus considerably reduced to as narrow as 12 meV. The coexistence of the resonant electron and the relaxed electron requires the emission of two electrons, which can occur through the exchange interaction.

1. Introduction

In quantum mechanics, two cases are considered in the model of a square potential well. One case is quantum confinement, in which the particle energy is lower than the well depth. The wave function of a particle in the well is a standing wave, and its energy states are quantized. The other case is quantum scattering, in which a free particle is scattered by the well. Because of the wave nature, only particles with specific energies can pass through the well without reflection; this is called resonance transmission. In reality, quantum confinement and quantum scattering can be observed in metallic films whose electronic structures have free-electron properties.[1–10] Herein, we report a new case called quantum trapping, in which a particle is in the well but has energy higher than the well depth. In this case, the particle can be temporarily trapped in the well; however, it can eventually escape from the well because of wave function dissipation. The mean duration for which the well traps the particle varies with the well size in oscillation. We demonstrate that quantum trapping can be experimentally revealed through the linewidth of the field emission resonance (FER)[11,12] observed

on the surface of bulk MoS$_2$ by using scanning tunneling microscopy (STM).

FER is a phenomenon in which electrons emitted from an STM tip due to a strong electric field enter the quantized standing wave state in the STM junction, becoming resonant electrons. Although the FER originates from the quantized states in a vacuum,[13] it can contain information associated with the physical properties of the surface and the STM tip. For example, FER energies can reveal the local work function of the surface.[14–20] FER intensities can reflect the local electron transmissivity of the reconstructed surface.[21] The zero valley intensities appearing around the FER may indicate that the observed material has a band gap above the vacuum level.[21] The number of FERs can manifest the sharpness[22–24] and field enhancement factor[25] of the STM tip. Previous studies have demonstrated that FER can be used to investigate the atomic structure of an insulator,[26] plasmon-assisted electron tunneling,[27] and the dynamics[28,29] and lateral quantization[30–32] of surface electrons above the vacuum level. In this study, we focus on the linewidth of the FER, which has seldom been investigated. The reciprocal of the linewidth can be interpreted as the mean lifetime of resonant electrons staying in the FER state, referring to a similar interpretation for quantum well states in metallic films.[3,4]

We discovered that the linewidth can modulate with the electric field of the forming FER and suggest that the oscillatory duration in quantum trapping is manifested by this linewidth modulation. The relationship between them is established by the following mechanisms. (1) The lifetime of a resonant electron only terminates with the occurrence of electron relaxation *via* light emission[22,33] because the bulk MoS$_2$ has a band gap

[a]Institute of Physics, Academia Sinica, Nankang, Taipei 11529, Taiwan. E-mail: wbsu@phys.sinica.edu.tw

[b]Department of Physics, National Tsing Hua University, Hsinchu 30013, Taiwan. E-mail: jeng@phys.nthu.edu.tw

[c]Physics Division, National Center for Theoretical Sciences, Hsinchu 30013, Taiwan

[d]Center for Condensed Matter Sciences, National Taiwan University, Taipei 10617, Taiwan

[e]Department of Physics, National Taiwan Normal University, Taipei 11677, Taiwan

† Electronic supplementary information (ESI) available. See DOI: 10.1039/d0na00682c

above the vacuum level. (2) Per unit time, two resonant electrons with opposite spins are successively emitted from the STM tip through the exchange interaction, and one resonant electron relaxes first. (3) Because of the inhomogeneous electric field resulting from the curvature of the STM tip, the electron relaxed from a resonant electron (named the relaxed electron) has lateral kinetic energy,[28] and a local potential well forms beneath the tip on the MoS_2 surface. Due to quantum trapping, the potential well temporarily traps the relaxed electron. When the potential well dimension matches the de Broglie wave length of the relaxed electrons, the mean trapping time that the potential well traps the relaxed electrons increases dramatically, manifesting resonance trapping. (4) Both the relaxed electron and the resonant electron have the same spin. According to the Pauli exclusion principle, the resonant electron cannot emit light while the relaxed electron remains trapped in the well, leading to the lifetime of this resonant electron being longer than that of the first one. Accordingly, the variation of the FER linewidth is mainly determined by the mean lifetime of resonant electrons relaxing subsequently.

2. Methods

2.1 STM measurements

A synthesized bulk Nb-doped MoS_2 sample (2D semiconductor) was cleaved in air using adhesive tape and then transferred into an ultrahigh vacuum STM operated at 78 K (bulk MoS_2 is an insulator at 5 K). FERs were observed by using a PtIr tip to perform Z–V spectroscopy under a current of 10 pA. Differentiation of the Z–V spectrum was executed using a numerical method to reveal FERs. It was not necessarily to immediately observe FERs when Z–V spectroscopy was performed. Whenever FERs did not appear, the method of applying a voltage pulse was used to improve the tip condition. Once FERs appeared on a clean area, we repeatedly took the spectra at different locations. Usually we could obtain hundreds of spectra before the FERs disappeared again. By inspecting the aspects of these spectra, we found that similar spectra could appear a few times. Then, the spectrum would spontaneously change into a different spectrum with FERs of disparate energies and shapes. Based on the similarity, hundreds of spectra could be divided into tens of groups. Similar spectra in each group were superposed to form one spectrum for analysis. The change of FER spectra originated from the spontaneous adjustment of the tip sharpness due to the high electric field at the tip apex and the thermal effect. Because the average period of the sharpness change was much longer than the acquisition time of taking one spectrum, we could obtain similar spectra with clear FERs before the sharpness changed and different spectra under different sharpness levels (see ESI note 1, Fig. S1†). By combining the spontaneous sharpness changes with the voltage pulses, spectra with FERs of different numbers were acquired.

2.2 DFT calculations

The electronic structures were calculated using the projector augmented wave (PAW) approach as implemented in the Vienna *Ab initio* Simulation Package (VASP) based on density functional theory (DFT). The Perdew–Burke–Ernzerhof (PBE) form of the generalized gradient approximation (GGA) was used for the exchange–correlation functional. The spin–orbit coupling was taken into account in the self-consistent field (SCF) calculations. For the bulk MoS_2 calculations, we used a 24 × 24 × 6 Monkhorst–Pack mesh for k-point sampling within the 3D Brillouin zone. A 24 × 24 × 1 Monkhorst–Pack k-mesh over the 2D Brillouin zone was adopted for the 3-layer MoS_2 slab calculations with a vacuum thickness of 15 Å well separating the slabs. The cutoff energy for the plane wave basis was set as 280 eV. The energy convergence threshold was set as 10^{-4} eV in the SCF calculations, while the energy convergence threshold was set as 10^{-3} eV for the structure optimizations. The electric field-induced valence electron density redistribution was studied by applying a uniform external electric field ranging from 0.0 to 0.3 V Å^{-1} along the normal to the plane of the MoS_2 slab. The out-of-plane charge profile was then obtained by summing the charge density over all grid points for each slice along the plane normal of the MoS_2 slab.

3. Results and discussion

3.1 The linewidth of the FER on MoS_2

Fig. 1(a) shows a differential Z–V spectrum with five FER peaks observed on a MoS_2 surface whose topographic image is displayed in the inset. The numbers represent the orders of the FER peaks. A previous study noted that the potential of the zeroth-order peak is the superposition of the image potential and the external potential, whereas that of higher-order peaks is simply the external potential.[14] Thus, the higher-order numbers are also the quantum numbers of quantized states in the external potential. The dashed line in Fig. 1(a) indicates the zero spectral intensity. The intensities of the valleys (marked by arrows) around the FER 2 peak are exactly zero, implying that MoS_2 has a band gap above the vacuum level in its projected bulk band structure and that the energy of FER 2 is in this band gap.[21]

Fig. 1(b) displays the FERs with numbers of three, four, five, and six. Recent studies have explained that under the same current, more FERs result from a sharper STM tip.[22–24] Fig. 1(b) also shows that the higher-order peaks in the spectra with three and five FERs are all much narrower than those in the spectra with four and six FERs. This phenomenon inspired us to explore the physics behind the linewidth of the higher-order FERs. Because of the zero valley intensities, the FER 2 peak is the most appropriate for analyzing the linewidth. Fig. 1(c)–(f) depict the Lorentzian fittings of FER 2 in Fig. 1(b). The linewidths extracted from the fittings modulate with the number of FERs, and the variation can be up to one order of magnitude. In particular, the linewidth can be as narrow as 12 meV for the case of five FERs. Statistic results show that about 10% of observed linewidths are below 20 meV. This linewidth modulation can also be observed on Ag(100) surface with a band gap above the vacuum level (see ESI note 2, Fig. S2†).[34] On the contrary, the linewidth modulation vanishes on Ag(111) without a band gap above the vacuum level (see ESI note 3, Fig. S3†).[34]
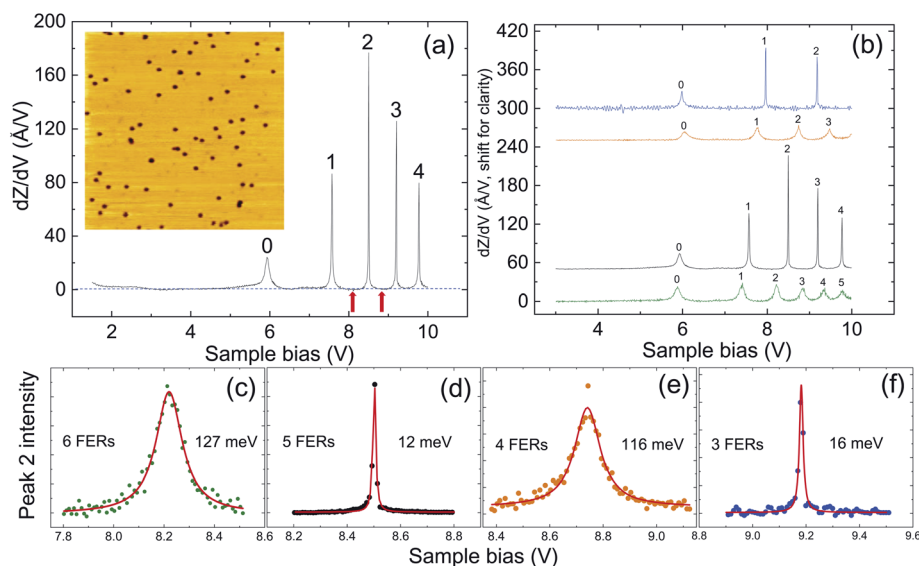
Fig. 1 (a) Differential $Z-V$ spectrum with five FER peaks marked by numbers. The zero spectral intensity is indicated by a dashed line, revealing that the intensities of the valleys (marked by arrows) around the FER 2 peak are zero. Inset: A typical STM image of the MoS_2 surface. The image size is 100 nm × 100 nm. (b) Differential $Z-V$ spectra with three, four, five, and six FERs. (c)–(f) Lorentzian fittings of FER 2 in (b). The linewidths extracted from the fittings modulate with the number of FERs.

Fig. 2(a) illustrates that an STM tip mainly consists of a base with an effective radius (typically a few tens of nanometers) and a protrusion (marked by the arrow). The sharpness of an STM tip is determined by the open angle of the protrusion.[24] According to electrostatics, the electric field in an STM junction is not constant due to the tip structure similar to that in
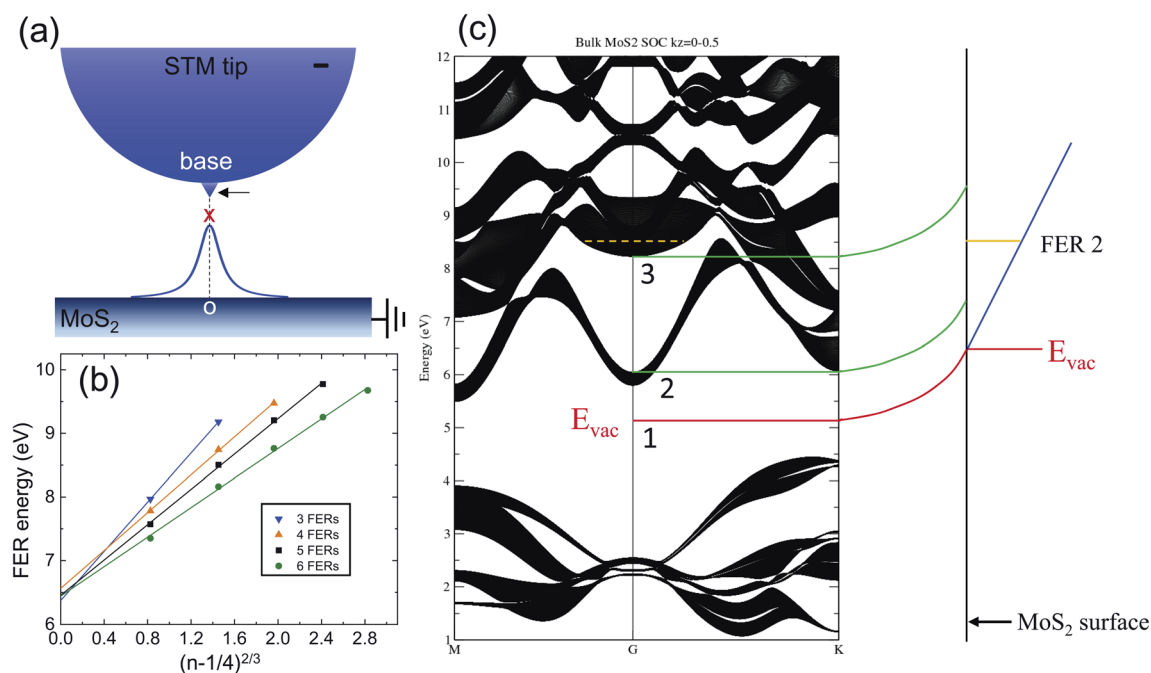

Fig. 2 (a) Illustration of an STM tip consisting of a base with a radius typically tens of nanometers and a protrusion (marked by the arrow). The electric field for FERs appears at the dashed line normal to the surface from the o point to the classical turning point (cross) of the resonant electron. Because of this tip structure, the electric potential below the classical turning point has a distribution curve. (b) Energies of the higher-order peaks in Fig. 1(b) versus $(n-1/4)^{2/3}$, showing the linear relationship, from which the electric fields for generating FERs of different numbers and vacuum levels can be acquired. (c) Projected bulk band structure of MoS_2 obtained by DFT calculation for energies ranging from 1 to 12 eV above the Fermi level. Line 1 indicates the vacuum level. Lines 2 and 3 mark the band edges of a band gap. The energy diagram on the right-hand side shows that due to band bending, the band edges and vacuum level in the bulk all move upward when approaching the surface.

Fig. 2(a). The field is the strongest at the tip but decays with distance from it.[23] As a result, the external potential in the vacuum above the Fermi level of the tip is steeper than that below the Fermi level along the surface normal. The former determines the tunneling probability of an electron at the Fermi level in the field emission, corresponding to an average electric field F_{FE}. The latter determines the number and energies of FERs, corresponding to an average electric field F_{FER}. The tip sharpness leads to the F_{FE} for field emission being stronger than the F_{FER} for FERs,[24] and a tip with higher sharpness can generate more FERs (see ESI note 4 for details†).

If an FER is a result of a quantized state in a triangular potential, then its energy E_n obeys[35]

$$E_n = E_{vac} + \alpha F_{FER}^{\frac{2}{3}} \left(n - \frac{1}{4} \right)^{\frac{2}{3}}, \quad (1)$$

where E_{vac} is the vacuum level, $n = 1, 2, 3\ldots$ is the quantum number, and

$$\alpha = \left(\frac{\hbar^2}{2m} \right)^{\frac{1}{3}} \left(\frac{3\pi e}{2} \right)^{\frac{2}{3}}. \quad (2)$$

Fig. 2(b) shows plots of the energies of the higher-order peaks in Fig. 1(b) *versus* $(n - 1/4)^{2/3}$. The results show that the data points in the cases of four, five, and six FERs can be fit well by the lines, indicating that eqn (1) is valid for higher-order peaks. From the line slope and the extrapolated value, one can obtain F_{FER} and E_{vac}, respectively. Fig. 2(b) reveals that a higher number of FERs corresponds to a weaker F_{FER}. Therefore, the modulated linewidth originates from the variation in F_{FER}.

3.2 Band bending in MoS$_2$

The F_{FER} obtained from Fig. 2(b) appears at the dashed line normal to the surface in Fig. 2(a) from the surface (0 point) to the classical turning point (cross) of the resonant electron. Because MoS$_2$ is a dielectric material with a dielectric constant of 3.7,[36] the electric field can penetrate its surface to cause band bending in the interior.[37] Thus, the electric potential along the surface normal is $V_b + F_{FER}z$, where V_b is the potential of band bending and z is the distance from the surface. The electric potential U_L below the classical turning point can be expressed as[28]

$$U_L(\rho, z) = \frac{(V_b + F_{FER}z)}{\left[1 + \left(\frac{\rho}{\rho_0} \right)^2 \right]}, \quad (3)$$

where ρ_0 is a constant and ρ is the lateral distance from the dashed line, corresponding to the distribution curve in Fig. 2(a). Fig. 2(c) displays the projected bulk band structure of MoS$_2$ obtained by DFT calculations[38–42] for energies within the range of 1–12 eV above the Fermi level. The result shows that a band gap appears above the vacuum level (5.2 eV),[43] which has band edges at 6.1 and 8.2 eV at the gamma point, marked by lines 2 and 3, respectively. Thus, the calculation result is consistent with the observation of the zero valley intensity in Fig. 1(a).

However, the energy of FER 2 in Fig. 1(a) is 8.5 eV, outside of the band gap marked by the dashed line in Fig. 2(c). This inconsistency can be attributed to band bending because the vacuum level determined from the extrapolation in Fig. 2(b) is 6.45 eV for the case of five FERs. The potential energy of band bending is accordingly determined to be 1.25 eV (6.45 eV − 5.2 eV). The energy diagram on the right-hand side of Fig. 2(c) illustrates that the band edges and the vacuum level (line 1) in the bulk all move upward when approaching the surface due to band bending. Therefore, the band edges at the surface are 7.35 and 9.45 eV. Consequently, the energy of FER 2 is in the band gap, in agreement with the observation.

3.3 Potential well on the MoS$_2$ surface under the STM tip

In addition to band bending, the penetration of the electric field can induce the positive polarization charge on the MoS$_2$ surface. By using eqn (3), the electric field $F_s(\rho)$ on the surface in the direction normal to the surface can be calculated as $F_{FER}/[1 + (\rho/\rho_0)^2]$. Then, the density of the polarization charge $\sigma(\rho)$ is calculated as

$$\sigma(\rho) = \frac{\varepsilon_0 (\varepsilon_r - 1) F_s}{\varepsilon_r}, \quad (4)$$

where ε_r is the dielectric constant of MoS$_2$. Fig. 3(a) shows the calculated density distribution of the polarization charge, displaying that the density is highest at the center and decreases with ρ. An electron on the surface under the STM tip is repelled by the electric field in vacuum but is also simultaneously attracted by the polarization charge. Consequently, the electric potential on the surface is the superposition of $U_L(\rho, 0)$ and the potential $U_p(\rho)$ due to the polarization charge. Because U_L and U_p are both zero when ρ is infinite, whether the electron faces a potential well can be determined from the sign of the resultant potential U_r at the 0 point, that is, $U_L(0, 0) + U_p(0)$. $U_L(0, 0)$ is the potential of band bending V_b, and $U_p(0)$ can be calculated as

$$U_p(0) = - \int_0^\infty \frac{\sigma(\rho) 2\pi\rho d\rho}{4\pi\varepsilon_0 \rho}, \quad (5)$$

where ρ_0 is the only parameter needed to calculate U_r. Fig. 3(b) shows U_r *versus* ρ_0 under the electric fields obtained from Fig. 2(b). The results indicate that U_r is negative for ρ_0 greater than 18 Å. The parameter ρ_0 is generally related to the tip base with an effective radius of tens of nanometers; therefore, it is plausible that ρ_0 is greater than 18 Å. Accordingly, U_r is negative, and a potential well exists on the MoS$_2$ surface beneath the STM tip. Moreover, U_r negatively increases with increasing F_{FER} for the same ρ_0, indicating that the depth of the potential well is deeper under a stronger F_{FER}.

Fig. 3(c) displays the calculated valence band partial charge profiles along the z-direction of the 3-layer MoS$_2$ slab under a uniform out-of-plane electric field (E_z) ranging from 0.0 to 0.3 V Å^{-1}. As clearly seen, the external electric field significantly modifies the surface MoS$_2$ layer valence charge profile by pulling electrons from the upper MoS$_2$ layer toward the lower MoS$_2$ layer, keeping the middle MoS$_2$ layer nearly neutral. As a result, the lower MoS$_2$ layer is negatively charged, whereas the upper
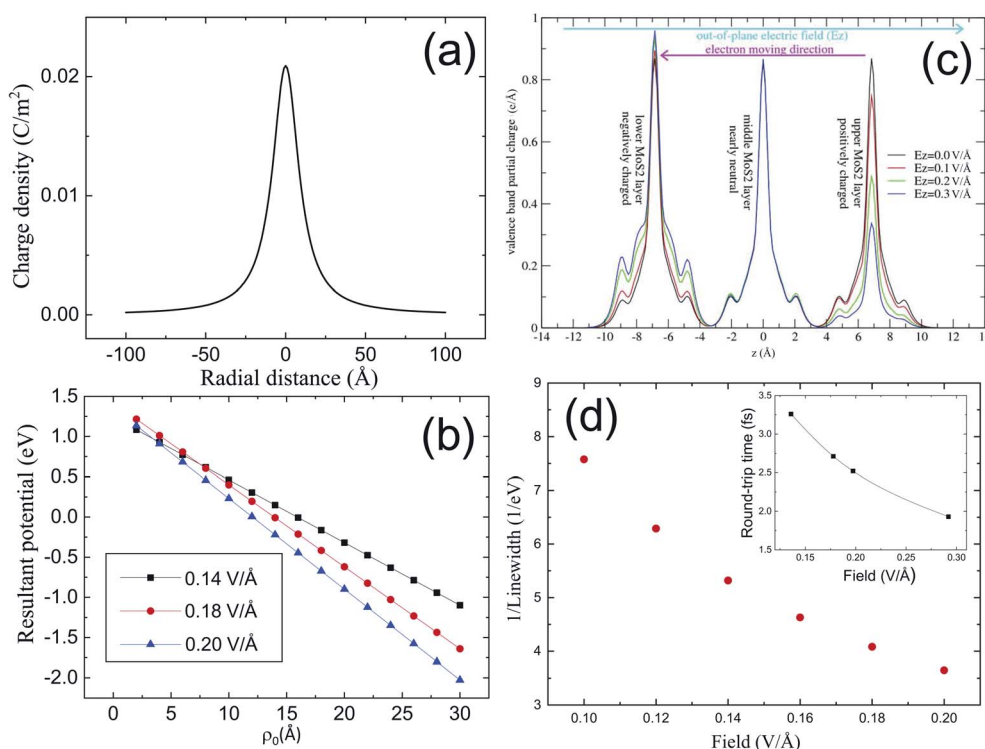
Fig. 3 (a) Calculated density distribution of the polarization charge under an electric field of 0.18 V Å^{-1} and $\rho_0 = 10$ Å, indicating that the density is the highest at the center and decreases with ρ. (b) Resultant potential U_r at the 0 point in Fig. 2(b) *versus* ρ_0 under electric fields obtained from Fig. 2(a). (c) Charge profile of the valence band of the MoS_2 slab under a uniform out-of-plane electric field ranging from 0.0 to 0.3 V Å^{-1}. The external electric field significantly modifies the surface MoS_2 trilayer valence charge profile. (d) The reciprocal of the FER linewidth of the first order *versus* the electric field, obtained from the calculation in ESI note 5.† Inset: RT time of a resonant electron in the STM junction *versus* the electric field obtained from Fig. 2(a).

MoS_2 layer is positively charged, consistent with our expectation. The electric field-induced electron transfer monotonically grows with increasing electric field strength, forming a mechanism for manipulating the width and depth of the potential well on the MoS_2 surface *via* the electric field in the STM junction. We note here that the calculated charge density of the surface MoS_2 layer is of the same order of magnitude as the maximum charge density estimated in Fig. 3(a).

3.4 Quantum trapping in one-dimensional square well

In the FER, resonant electrons move back and forth within a specific distance between the surface and the classical tuning point. Because E_n, F_{FER}, and E_{vac} are known, this distance s corresponding to FER can be calculated as $(E_n - E_{vac})/eF_{FER}$. Consequently, the round-trip (RT) time t for resonant electron motion can be calculated from $2s = eF_{FER}t^2/m$. The inset in Fig. 3(d) shows the RT time *versus* F_{FER} in the case of FER 2, where the RT time is shown on the femtosecond scale. Previous studies have demonstrated that resonant electrons can emit light[22,33] to become relaxed electrons with a lateral kinetic energy due to the inhomogeneous field in the STM junction;[28] however, before relaxation, electrons should complete at least one RT to form the standing wave necessary to reveal the FER. Therefore, the RT time can basically reflect the lifetime of the resonant electrons. Thus, the inset in Fig. 3(d) indicates that the

lifetime should monotonically decrease with increasing F_{FER}, which can also be confirmed by exploiting the Fabry–Pérot mode[2] to calculate the reciprocal of the FER linewidth of the first order without including the light emission and the band structure of the sample (see ESI note 5 for details†), as shown in Fig. 3(d). Fig. 3(d) is evidently contradictory to the observation in Fig. 1 that the linewidth modulates with F_{FER}. The modulation range can be as large as one order of magnitude, implying that under a certain F_{FER}, the lifetime can be substantially prolonged. Because the lifetime of a resonant electron terminates upon light emission, this significant extension of the lifetime indicates that resonant electrons cannot emit light to remain in FER for many more RTs. We suggest that the prohibition of light emission results from the same spin of the relaxed electron and the resonant electron as well as the Pauli exclusion principle.

The linewidth of 12 meV corresponds to a lifetime of 27 fs if $\Delta E \Delta t = \hbar/2$. Therefore, the intervention of the Pauli exclusion principle requires a resonant electron and a relaxed electron to coexist on the femtosecond time scale. However, the set current in our experiment is 10 pA, which is equal to one electron per 16 ns. If electrons are emitted one by one every 16 ns, then two electrons cannot coexist on the femtosecond scale. In this context, we suggest that every 32 ns, two resonant electrons with opposite spins are successively emitted into the quantized state

in the FER (Fig. 4(a)), which can occur through the exchange interaction (see ESI note 6 for details†). One resonant electron relaxes first through light emission and its spin should flip during relaxation to maximize the total spin according to Hund's rule. Consequently, the resonant electron and relaxed electron can simultaneously exhibit the same spin (Fig. 4(b)). The forbiddance of light emission from the resonant electron is accordingly established. The situation of the same spin in Fig. 4(b) is similar to the triplet excited state in phosphorescence.

Because the resonant electrons are hot electrons, the lateral kinetic energy E of relaxed electrons is higher than the vacuum level of MoS_2. Therefore, relaxed electrons in the potential well have energy higher than the well depth, which differs from the case of quantum confinement. One can expect that relaxed electrons are trapped such that they move back and forth in the well because of the formation of standing waves in the radial direction. However, these standing waves will dissipate because the wave function outside the well is a traveling wave instead of an evanescent wave. Therefore, relaxed electrons eventually leave the well. To model this case of quantum trapping, we assume that the potential well is a cylindrical well in which the radial wave function is a Bessel function of the first kind. We note that Bessel functions have oscillatory features similar to cosinusoidal and sinusoidal functions; this enables us to

discuss quantum trapping by using a one-dimensional square well with depth V_0 and width $2L$, as depicted in Fig. 4(c). The wave vector k of the relaxed electrons in the well satisfies

$$kL = \beta L \sqrt{1 + \frac{E}{V_0}}, \tag{6}$$

where $\beta = \frac{\sqrt{2mV_0}}{\hbar}$. The formation of standing waves requires the relaxed electrons to be reflected at $-L$ and L so that they go through a complete cycle in the square well. If the energy of relaxed electrons is much higher than the well depth ($E \gg V_0$), then these electrons behave similarly to classical particles and leave the well without reflection. Accordingly, the wave function of relaxed electrons after the first cycle can be

$$\psi_1(x) = e^{-\gamma E} \frac{\cos kx}{\sqrt{L}} \tag{7}$$

or

$$\psi_2(x) = e^{-\gamma E} \frac{\sin kx}{\sqrt{L}}, \tag{8}$$

where γ is a constant. The exponential term can satisfy no standing wave for $E \gg V_0$ because E can be considered infinite under this condition. Thus, the probability in the well is

$$P_1 = \int_{-L}^{L} \psi_1^2 \mathrm{d}x = e^{-2\gamma E}\left(1 + \frac{\sin 2kL}{2kL}\right) \tag{9}$$

or

$$P_2 = \int_{-L}^{L} \psi_2^2 \mathrm{d}x = e^{-2\gamma E}\left(1 - \frac{\sin 2kL}{2kL}\right). \tag{10}$$

when $E = 0$ and $0 < 2kL < \pi$, $\sin 2kL$ is positive, and thus $P_1 > 1$ and $P_2 < 1$. Because the probability should not be greater than 1, the wave function is $\psi_2(x)$ in this case. Similarly, the wave function is $\psi_1(x)$ when $E = 0$ and $\pi < 2kL < 2\pi$.

The results in Fig. 3(b) indicate that V_0 and β can increase with F_{FER}. Moreover, the area with polarization charges is larger under a stronger F_{FER}. Hence, L is wider when F_{FER} is higher. Consequently, the well size $2LV_0$ can be tuned by F_{FER}. Based on eqn (3), the electrostatic force in the radial direction enhances with F_{FER}, causing E to also increase with F_{FER}. Therefore, it is plausible to calculate the probability under the conditions that E/V_0 is a constant independent of F_{FER} and E is replaced with βL. By combining eqn (9) and (10), the probability $P(1)$ that a relaxed electron exists in the well after the first cycle can be expressed as

$$P(1) = e^{-2\gamma\beta L}\left(1 - \left|\frac{\sin 2kL}{2kL}\right|\right). \tag{11}$$

Therefore, the probability of leaving the well is $1 - P(1)$, which can be viewed as the decay rate R of the probability. Accordingly, the probability that a relaxed electron stays in the well for h cycles is

$$P(h) = (1 - R)^h. \tag{12}$$

From eqn (12), we know that the probability that a relaxed electron has remained in the well for $(h - 1)$ cycles but leaves
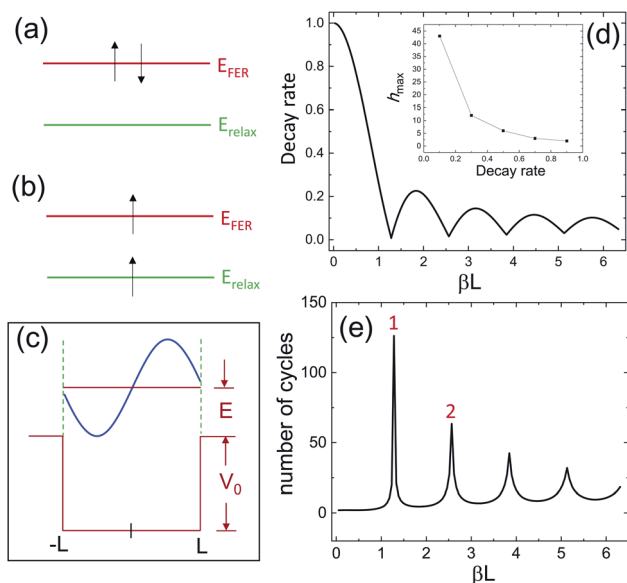

Fig. 4 (a) Two electrons with opposite spins are successively emitted into the quantized state in FER. (b) When one of the resonant electrons in (a) relaxes, its spin should be flipped to maximize the total spin according to Hund's rule. (c) One-dimensional square potential well with a width of $2L$ for modeling the quantum trapping, where the energy E of the relaxed electron in the well is higher than the well depth V_0 and the wave function of the relaxed electron is a standing wave. (d) Decay rate of the probability *versus* βL, which is proportional to the size of the well, revealing local minima for $E/V_0 = 0.5$ and $\gamma = 0.003$. Inset: Maximum number of cycles $h_{\max}$ for which the relaxed electron can remain in the well as a function of the decay rate for $N = 100$. (e) Average number of cycles *versus* βL showing an oscillatory feature; the maxima occur exactly at the minima of the decay rate in (d).

the well in the hth cycle is $P(h-1)-P(h)$. As a result, the average number of cycles $\bar{h}$ of all relaxed electrons is

$$\bar{h} = \sum_{h=0}^{h=h_{max}} h[P(h) - P(h+1)], \qquad (13)$$

where h_{max} is the maximum number of cycles for which a relaxed electron can remain, which depends on the number N of all relaxed electrons when observing the FER.

Eqn (11) indicates that $P(1)$ depends only on βL; this enables us to show the decay rate versus βL. Fig. 4(d) demonstrates that the decay rate varies with βL in oscillation, and a local minimum appears when $2kL$ equals an integral multiple of π. The manifestation of local minima is due to the transition of the wave function. The inset in Fig. 4(d) shows h_{max} as a function of the decay rate, revealing that h_{max} increases with decreasing decay rate. Consequently, when the decay rate is lower, the average number of cycles should be higher because relaxed electrons can remain in the well for more cycles. We use the results in Fig. 4(d) and eqn (12) and (13) to calculate the average number of cycles $\bar{h}$ versus βL. Fig. 4(e) shows that $\bar{h}$ oscillates with βL, and the maxima occur exactly at the minima of the decay rate. In addition, $\bar{h}$ is insensitive to N.

The time per cycle, equal to $4L/(\hbar k/m)$, is proportional to L/β. Because both β and L increase with F_{FER}, it is plausible that the cycle time is independent of F_{FER}. Because βL is proportional to the well size, Fig. 4(e) can be interpreted as evidence that the mean duration for which the square well traps relaxed electrons oscillates with the well size. For certain sizes, the mean trapping time (MTT) is much longer, manifesting resonance trapping. The MTT can change by up to one order of magnitude at the first and second resonances marked by 1 and 2 in Fig. 4(e), respectively. Evidently, the variation in the linewidths in Fig. 1(c)–(f) has the characteristics of quantum trapping, leading us to suggest that the lifetime of a resonant electron is governed by the relaxed electron through the Pauli exclusion principle. Thus, the MTT is recorded in the linewidth of the FER. The narrow linewidths of 12 meV and 16 meV in Fig. 1(d) and (f), respectively, result from the relaxed electrons

engaging in resonance trapping. Broad FERs indicate low MTT in quantum trapping. Due to quantum trapping, the lifetimes of paired resonant electrons in Fig. 4(a) can be different. The variation in the FER linewidth is mainly determined by the mean lifetime of resonant electrons relaxing subsequently. Moreover, we have also accumulated sufficient spectra with four, five and six FERs to plot the reciprocal of the linewidth versus F_{FER} to display resonance trapping, as shown in Fig. 5. The plot displays that F_{FER} could be gradually increased from 0.13 to 0.23 V Å^{-1}. The plot depicts the characteristics of a narrow peak, which are highly similar to the peak of resonance trapping in Fig. 4(e). Therefore, Fig. 5 demonstrates that the resonance trapping only appeared under a certain F_{FER}, which is 0.178 V Å^{-1} (marked by a dashed line). However, at approximately 0.178 V Å^{-1}, several data points still appear with values are close to those at 0.14 and 0.22 V Å^{-1}. Fig. 4(e) displays that the resonance trapping is highly sensitive to the size of the potential well. Therefore, the appearance of these data points indicates that even when the electric fields are near 0.178 V Å^{-1}, their corresponding tip structures may induce potential wells with sizes that deviate slightly from those for resonance trapping, causing a low $1/\Delta E$. In addition, the data points in Fig. 5 are colored in terms of the number of FERs. It is clear that the high values of $1/\Delta E$ appear at 5 FERs, whereas the values of $1/\Delta E$ are low for 4 and 6 FERs.

4. Conclusions

In summary, we discover that the linewidth of the FER is a meaningful quantity that is not only associated with the lifetime of a resonant electron but is also able to store information regarding the behavior of relaxed electrons. The delivery of information occurs through the action of the Pauli exclusion principle. In this study, when the size of the potential well on the MoS_2 surface situates the relaxed electrons in resonance trapping, the resonant electrons can receive this information such that their lifetimes are considerably extended. Therefore, ultra-narrow FERs are manifested. Furthermore, the potential well induced by the STM tip should be generally formed on the surfaces of different materials, implying that the phenomenon of quantum trapping can be universally observed. The variation in the well size with the electric field may depend on the dielectric properties of the materials. Therefore, quantum trapping manifested in the STM configuration can be developed as a new technique for probing dielectric properties on the nanometer scale.

Conflicts of interest
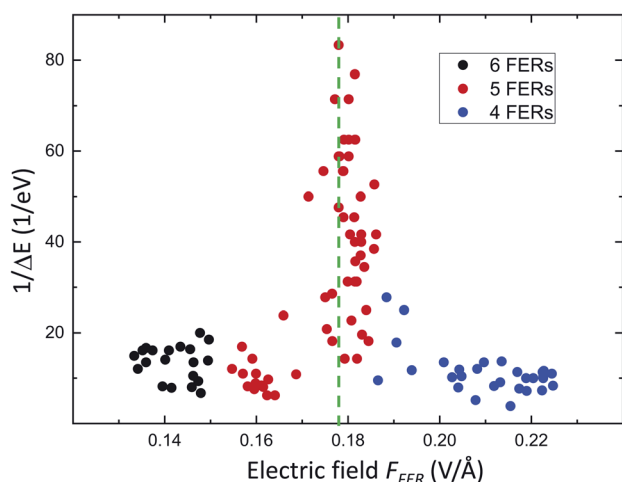
There are no conflicts to declare.

Acknowledgements

Fig. 5 Plot of $1/\Delta E$ versus F_{FER}, in which the data points are accumulated from 108 spectra with four, five, and six FERs.

References

1 I. B. Altfeder, K. A. Matveev and D. M. Chen, Electron fringes on a quantum wedge, *Phys. Rev. Lett.*, 1997, **78**, 2815–2818.

2 J. J. Paggel, T. Miller and T. C. Chiang, Quantum-well states as Fabry-Perot modes in a thin-film electron interferometer, *Science*, 1999, **283**, 1709–1711.

3 M. Becker and R. Berndt, Scattering and lifetime broadening of quantum well states in Pb films on Ag(111), *Phys. Rev. B: Condens. Matter Mater. Phys.*, 2010, **81**, 205438.

4 D. Wegner, A. Bauer and G. Kaindl, Electronic structure and dynamics of quantum-well states in thin Yb metal films, *Phys. Rev. Lett.*, 2005, **94**, 126804.

5 M. C. Yang, C. L. Lin, W. B. Su, S. P. Lin, S. M. Lu, H. Y. Lin, C. S. Chang, W. K. Hsu and T. T. Tsong, Phase Contribution of image potential on empty quantum well states in Pb islands on the Cu(111) surface, *Phys. Rev. Lett.*, 2009, **102**, 196102.

6 J. Kim, S. Qin, W. Yao, Q. Niu, M. Y. Chou and C. K. Shih, Quantum size effects on the work function of metallic thin film nanostructures, *Proc. Natl. Acad. Sci. U. S. A.*, 2010, **107**, 12761–12765.

7 W. Y. Chan, H. S. Huang, W. B. Su, W. H. Lin, H. T. Jeng, M. K. Wu and C. S. Chang, Field-induced expansion deformation in Pb Islands on Cu(111): evidence from energy shift of empty quantum-well states, *Phys. Rev. Lett.*, 2012, **108**, 146102.

8 J. A. Kubby, Y. R. Wang and W. J. Greene, Electron interferometry at a heterojunction interface, *Phys. Rev. Lett.*, 1990, **65**, 2165.

9 W. F. Chung, Y. J. Feng, H. C. Poon, C. T. Chan, S. Y. Tong and M. S. Altman, Layer spacings in coherently strained epitaxial metal films, *Phys. Rev. Lett.*, 2003, **90**, 216105.

10 W. B. Su, S. M. Lu, C. L. Jiang, H. T. Shih, C. S. Chang and T. T. Tsong, Stark shift of transmission resonance in scanning tunneling spectroscopy, *Phys. Rev. B: Condens. Matter Mater. Phys.*, 2006, **74**, 155330.

11 G. Binnig, K. H. Frank, H. Fuchs, N. Garcia, B. Reihl, H. Rohrer, F. Salvan and A. R. Williams, Tunneling spectroscopy and inverse photoemission - image and field states, *Phys. Rev. Lett.*, 1985, **55**, 991–994.

12 R. S. Becker, J. A. Golovchenko and B. S. Swartzentruber, Electron interferometry at crystal-surfaces, *Phys. Rev. Lett.*, 1985, **55**, 987–990.

13 K. H. Gundlach, Zur Berechnung Des Tunnelstroms Durch Eine Trapezformige Potentialstufe, *Solid-State Electron.*, 1966, **9**, 949–957.

14 C. L. Lin, S. M. Lu, W. B. Su, H. T. Shih, B. F. Wu, Y. D. Yao, C. S. Chang and T. T. Tsong, Manifestation of work function difference in high order Gundlach oscillation, *Phys. Rev. Lett.*, 2007, **99**, 216103.

15 H. S. Huang, W. Y. Chan, W. B. Su, G. Hoffmann and C. S. Chang, Measurement of work function difference between Pb/Si(111) and Pb/Ge/Si(111) by high-order Gundlach oscillation, *J. Appl. Phys.*, 2013, **114**, 214308.

16 F. Schulz, R. Drost, S. K. Hämäläinen, T. Demonchaux, A. P. Seitsonen and P. Liljeroth, Epitaxial hexagonal boron nitride on Ir(111): A work function template, *Phys. Rev. B: Condens. Matter Mater. Phys.*, 2014, **89**, 235429.

17 Z. Li, H. Y. Chen, K. Schouteden, E. Janssens, C. Van Haesendonck, P. Lievens and G. Pacchioni, Spontaneous doping of two-dimensional NaCl films with Cr atoms: aggregation and electronic structure, *Nanoscale*, 2015, **7**, 2366.

18 K. Schouteden, B. Amin-Ahmadi, Z. Li, D. Muzychenko, D. Schryvers and C. Van Haesendonck, Electronically decoupled stacking fault tetrahedra embedded in Au(111) films, *Nat. Commun.*, 2016, **7**, 14001.

19 C. Gutiérrez, L. Brown, C. J. Kim, J. Park and A. N. Pasupathy, Klein tunneling and electron trapping in nanometre-scale graphene quantum dots, *Nat. Phys.*, 2016, **12**, 3806.

20 Q. Zhang, J. Yu, P. Ebert, C. Zhang, C. R. Pan, M. Y. Chou, C. K. Shih, C. Zeng and S. Yuan, Tuning Band gap and work function modulations in monolayer hBN/Cu(111) heterostructures with moire patterns, *ACS Nano*, 2018, **12**, 9355.

21 W. B. Su, S. M. Lu, C. L. Lin, H. T. Shih, C. L. Jiang, C. S. Chang and T. T. Tsong, Interplay between transmission background and Gundlach oscillation in scanning tunneling spectroscopy, *Phys. Rev. B: Condens. Matter Mater. Phys.*, 2007, **75**, 195406.

22 J. Martínez-Blanco and S. Fölsch, Light emission from Ag(111) driven by inelastic tunneling in the field emission regime, *J. Phys.: Condens. Matter*, 2015, **27**, 255008.

23 W. Y. Chan, S. M. Lu, W. B. Su, C. C. Liao, G. Hoffmann, T. R. Tsai and C. S. Chang, Sharpness-induced energy shifts of quantum well states in Pb islands on Cu(111), *Nanotechnol*, 2017, **28**, 095706.

24 S. M. Lu, W. Y. Chan, W. B. Su, W. W. Pai, H. L. Liu and C. S. Chang, Characterization of external potential for field emission resonances and its applications on nanometer-scale measurements, *New J. Phys.*, 2018, **20**, 043014.

25 W. B. Su, C. L. Lin, W. Y. Chan, S. M. Lu and C. S. Chang, Field enhancement factors and self-focus functions manifesting in field emission resonances in scanning tunneling microscopy, *Nanotechnol*, 2016, **27**, 175705.

26 K. Bobrov, A. J. Mayne and G. Dujardin, Atomic-scale imaging of insulating diamond through resonant electron injection, *Nature*, 2001, **413**, 616–619.

27 S. Liu, M. Wolf and T. Kumagai, Plasmon-assisted resonant electron tunneling in a scanning tunneling microscope junction, *Phys. Rev. Lett.*, 2018, **121**, 226802.

28 J. I. Pascual, C. Corriol, G. Ceballos, I. Aldazabal, H. P. Rust, K. Horn, J. M. Pitarke, P. M. Echenique and A. Arnau, Role of the electric field in surface electron dynamics above the vacuum level, *Phys. Rev. B: Condens. Matter Mater. Phys.*, 2007, **75**, 165326.

29 P. Wahl, M. A. Schneider, L. Diekhoner, R. Vogelgesang and K. Kern, Quantum coherence of image-potential states, *Phys. Rev. Lett.*, 2003, **91**, 106802.

30 K. Schouteden and C. Van Haesendonck, Quantum confinement of hot image-potential state electrons, *Phys. Rev. Lett.*, 2009, **103**, 266805.

31 S. Stepanow, A. Mugarza, G. Ceballos, P. Gambardella, I. Aldazabal, A. G. Borisov and A. Arnau, Localization, splitting, and mixing of field emission resonances induced by alkali metal clusters on Cu(100), *Phys. Rev. B: Condens. Matter Mater. Phys.*, 2011, **83**, 115101.

32 F. Craes, S. Runte, J. Klinkhammer, M. Kralj, T. Michely and C. Busse, Mapping Image Potential States on Graphene Quantum Dots, *Phys. Rev. Lett.*, 2013, **111**, 056804.

33 J. Coombs, J. Gimzewski, B. Reihl, J. Sass and R. Schlittler, Photon emission experiments with the scanning tunneling microscope, *J. Microsc.*, 1988, **152**, 325.

34 S. Schuppler, N. Fischer, Th. Fauster and W. Steinmann, Lifetime of image-potential states on metal surfaces, *Phys. Rev. B: Condens. Matter Mater. Phys.*, 1992, **46**, 13539.

35 J. J. Sakurai, *Modern Quantum Mechanics*, Benjamin-Cummings, New York, 1st edn, 1985, p. 104.

36 C. P. Lu, G. Li, K. Watanabe, T. Taniguchi and E. Y. Andrei, MoS_2: choice substrate for accessing and tuning the electronic properties of graphene, *Phys. Rev. Lett.*, 2014, **113**, 156804.

37 R. M. Feenstra, Y. Dong, M. P. Semtsiv and W. T. Masselink, Influence of tip-induced band bending on tunneling spectra of semiconductor surfaces, *Nanotechnol*, 2016, **18**, 044015.

38 G. Kresse and J. Furthmuller, Efficiency of *ab initio* total energy calculations for metals and semiconductors using a plane-wave basis set, *Comput. Mater. Sci.*, 1996, **6**, 15–50.

39 G. Kresse, *Ab initio* molecular dynamics for liquid metals, *J. Non-Cryst. Solids*, 1995, **192–193**, 222–229.

40 G. Kresse and J. Furthmuller, Efficient iterative schemes for *ab initio* total-energy calculations using a plane-wave basis set, *Phys. Rev. B: Condens. Matter Mater. Phys.*, 1996, **54**, 11169–11186.

41 J. P. Perdew, J. A. Chevary, S. H. Vosko, K. A. Jackson, M. R. Pederson, D. J. Singh and C. Fiolhais, Atoms, molecules, solids, and surfaces: applications of the generalized gradient approximation for exchange and correlation, *Phys. Rev. B: Condens. Matter Mater. Phys.*, 1992, **46**, 6671–6687.

42 J. P. Perdew and Y. Wang, Pair-distribution function and its coupling-constant average for the spin-polarized electron-gas, *Phys. Rev. B: Condens. Matter Mater. Phys.*, 1992, **46**, 12947–12954.

43 I. Popov, G. Seifert and D. Tomanek, Designing electrical contacts to MoS_2 monolayers: a computational study, *Phys. Rev. Lett.*, 2012, **108**, 156802.